Journal of Applied Polymer Science

Investigation on jet stability, fiber diameter, and tensile properties of electrospun polyacrylonitrile nanofibrous yarns

Bipul Barua, Mrinal C. Saha
School of Aerospace and Mechanical Engineering, University of Oklahoma, Norman, Oklahoma 73019
Correspondence to: M.C. Saha (E-mail: msaha@ou.edu)

ABSTRACT: Electrospinning is a flexible and efficient method for producing nanofibers by using relatively dilute polymer solution. However, there are many parameters related to material and processing that influence the morphology and property of the nanofibers. This study investigates the influence of electric field and flow rate on diameter and tensile properties of nanofibers produced using polyacrylonitrile (PAN)-dimethylformamide (DMF) solution. Stability of the spinning jet is investigated via fiber current measurement and an image system at different electric fields and solution flow rates. It is observed that a set of electric field and flow rate conditions favor producing thinnest, strongest, and toughest nanofibers during electrospinning process. Other conditions may lead to instability of the Taylor cone, discontinuous jet, larger diameter fiber, and lower mechanical properties. Finally, a simple dynamic whipping model is adopted to correlate the nanofiber diameter with volumetric charge density and is found to be excellent validating our experimental results. © 2015 Wiley Periodicals, Inc. J. Appl. Polym. Sci. **2015**, *132*, 41918.

KEYWORDS: electrospinning; fibers; properties and characterization

Received 27 October 2014; accepted 29 December 2014
DOI: 10.1002/app.41918

INTRODUCTION

The increasing demands on nanotechnology in every aspect of modern manufacturing lead to pioneering scientific research. The reduction of particle size from micrometers to nanometers brings several amazing characteristics such as high surface area, high surface energy, superior strength, and stiffness. Nanofibers are gaining significant attention in recent years as nanofillers for composite structures, supercapacitors, directional heat transfer, and energy storage applications. Among various techniques[1–7] available electrospinning appears to be the most straightforward and versatile technique for producing nanofibers using a wide range of polymer solutions.[8,9] In a typical electrospinning system, a high-voltage is applied to a polymer solution at the tip of an electrode and at sufficient voltage the electrostatic repulsion force prevails over the surface tension of the solution and triggers the formation of a jet in the form of a Taylor cone at the end of the solution droplet.[10,11] The polymer solution jet is expelled from the apex of the Taylor cone and accelerated toward the collector, which is usually grounded. The emitted charged jet usually travels few centimeters in a straight path due to a longitudinal stress caused by the external field. Then a lateral perturbation grows in response to the repulsive forces between adjacent elements of charge carried by the jet and initiates a whipping instability resulting in enormous stretching of the jet and formation of nanofiber.[10] During the flight, the polymer solution jet also experiences solvent evaporation and eventually deposits onto the collector as solid (or mostly solid) nanofiber. The collector can be designed for producing random, nonwoven mats, and aligned structures. Electrospun nanofibers have numerous potential applications such as high performance filters, sensors, biomaterial polymers, electrically conductive nanofibers, composites, and tissue scaffolds due to their high specific surface area, high porosity, and high absorption capacity.[8,12,13]

Despite the apparent simplicity of the electrospinning process, the process itself is quite complicated owing to many parameters that influence the morphology and diameter of electrospun fiber. The processing parameters include: (a) the intrinsic properties of the solution such as polymer concentration,[14,15] solution viscosity,[14,15] molecular weight,[14,16] conductivity,[9] and surface tension[17]; and (b) the operational conditions such as electrospinning voltage,[18,19] distance between spinneret and collector,[18,19] solution flow rate,[20] and collector geometry.[21] However, the effect of solution properties can be difficult to isolate since one parameter can generally affect other properties. For example, changing the viscosity of the solution can also change the conductivity.[22] In addition, environmental conditions such as humidity and temperature can affect the morphology and diameter of the electrospun nanofibers.[23,24]

Among many parameters, polymer concentration has been mostly investigated and also found to be the main factor for

controlling fiber diameter and morphology. At low polymer concentration, beading and droplets on the fiber surface have been reported[25,26]; the process under these conditions is predominantly characterized as electrospraying.[27] The increasing of the polymer concentration to a critical point leads to uniform and bead free fibers.[14,28] However, there seems to be a general agreement that the increase in the polymer concentration leads to increase in the fiber diameter due to higher number of entanglements between polymer chains, which oppose jet stretching under electric field. Both conductivity[29,30] and surface tension[17,31] of polymer solution have also been reported as influential parameters for electrospinning process. Generally, higher conductivity leads to thinner nanofibers and lower surface tension leads to less bead formation. Although the effects of solution parameters on diameter of the electrospun nanofiber are well established, the influence of the operational conditions such as electrospinning voltage and flow rate shows inconsistent results. Some studies showed that the diameter of the fiber decreases with increasing electrospinning voltage or field strength,[9,18,32,33] while others showed opposite trend.[34–36] In some studies, the relationship between nanofiber diameter and field strength was found ambiguous. For example, Yordem *et al.*[37] found that depending on the solution concentration and needle to collector distance the nanofiber diameter can increase, decrease, and initial decrease followed by increase with increasing electrospinning voltage. Careful observation of the data reported by Buchko *et al.*[38] revealed that the average diameter of electrospun nylon nanofibers decreased to a minimum value and then increased with increasing field strength. It is also noticed that the standard deviation was lower when the nanofiber diameter reached to the minimum value. Similarly, several authors showed that the diameter of the nanofiber increased with increasing the flow rate,[39,40] while others found no significant influence of the flow rate.[41,42] The effect of collector distance has not been reported to be significant,[43,44] although a minimum distance is required to ensure that the electrospun fibers have sufficient time to dry before reaching the collector.[43]

Reneker and Yarin[45] investigated the effect of flow rate and electric voltage on Taylor cone for stable electrospinning process. They found that the rate at which solution flows into the Taylor cone must be equal to the rate at which fluid is carried away by the jet to achieve a stable electrospinning process. They defined this condition as quasi-stable point which can be achieved by investigating the Taylor cone at the tip of the needle by adjusting either the applied voltage or the flow rate or both. Thus, higher flow rate is required at higher applied voltage for a stable electrospinning jet. Recently, Cai and Gevelber[46] have shown that a minimum fluctuation in the volume of the Taylor cone is required to maintain the electrospinning process stable for long time.

PAN has been found to be the most suitable and widely used precursor for producing high performance carbon microfibers.[47] The bulk of the production cost incurred during carbon fiber production is due to the prolonged heating required for the thermal conversion of the precursor fibers into structural carbon fibers. It is believed that the drawback of prolonged heating time can greatly be resolved if the fiber diameter is significantly reduced.[47] Moreover, reducing the fiber diameter increases the strength of carbon fiber by lowering the probability of encountering a critical flaw in a given test length.[48] Thus, the preparation of PAN nanofibers is of great interest to the scientists. Many researchers have worked on the electrospinning of PAN/DMF solution and have obtained electrospun PAN fibers with diameters in the range of 100–2700 nm depending on various electrospinning parameters.[37,49–52] While significant insights have been achieved, there is still inconsistency in the findings of the influence of electrospinning voltage and flow rate on the diameter of the PAN nanofiber.[37,49,50] The mechanical behavior of electrospun nanofibers is expected to differ from bulk and microscale fibers due to their fabrication process and large surface to-volume ratio. Papkov *et al.*[53] investigated the tensile property of individual electrospun PAN fibers for a large range diameters. Their results show that the reduction of nanofiber diameter from 2.8 μm to ~100 nm resulted in simultaneous increase in strength from 15 to 1750 MPa, and toughness from 0.25 to 605 MPa. While Papkov *et al.*[53] measured the property of the individual nanofiber; other researchers have used the tensile property of electrospun nanofiber mat or yarn as a characterization tool due to the requirement of expensive apparatus such as atomic force microscopy, nano UTM, nanomanipulator for single nanofiber test.[54] Moon and Harris[55] used the cross-sectional area of the yarn, which was calculated by dividing the mass of the yarn by its length and density of PAN, to determine the tensile property of the yarn. Their reported tensile strength of PAN nanofiber yarn with 431 nm average filament diameter was 99 MPa. Hou *et al.*[56] reported 45.7 MPa for PAN nanofiber mat with average filament diameter of ~200 nm.

In this study, we investigate the influence of solution flow rate and applied voltage on the diameter of electrospun polyacrylonitrile (PAN) nanofibers. We optically study the Taylor cone at the tip of the needle and monitor the fiber current to identify different flow regimes at different applied voltages. We investigate the influence of different flow regimes on jet stability and the resultant average fiber diameter and tensile properties of the PAN nanofiber yarns.

EXPERIMENTAL

Material

Polyacrylonitrile (PAN) with an average molecular weight of about 150,000 g/mol was used as polymer and *N,N*–dimethylformamide (DMF) was used as solvent to make polymer solution. Both polymer and solvent were purchased from Sigma-Aldrich. PAN polymer powder was dried at 100°C under vacuum for 2 h to remove any access moisture and then dissolved in DMF at 80°C using a magnetic stirrer to obtain the spinning solution. Any air bubbles entrapped into the solution were carefully purged prior to electrospinning.

Electrospinning Process

A schematic of a custom built electrospinning setup is shown in Figure 1. The spinning solution was prepared using 10% PAN (by weight) in DMF and fed using a vertical syringe pump via a stainless steel needle having 0.41 mm inner diameter. The needle was electrically connected to a positive high voltage DC power supply purchased from Spellman High Voltage

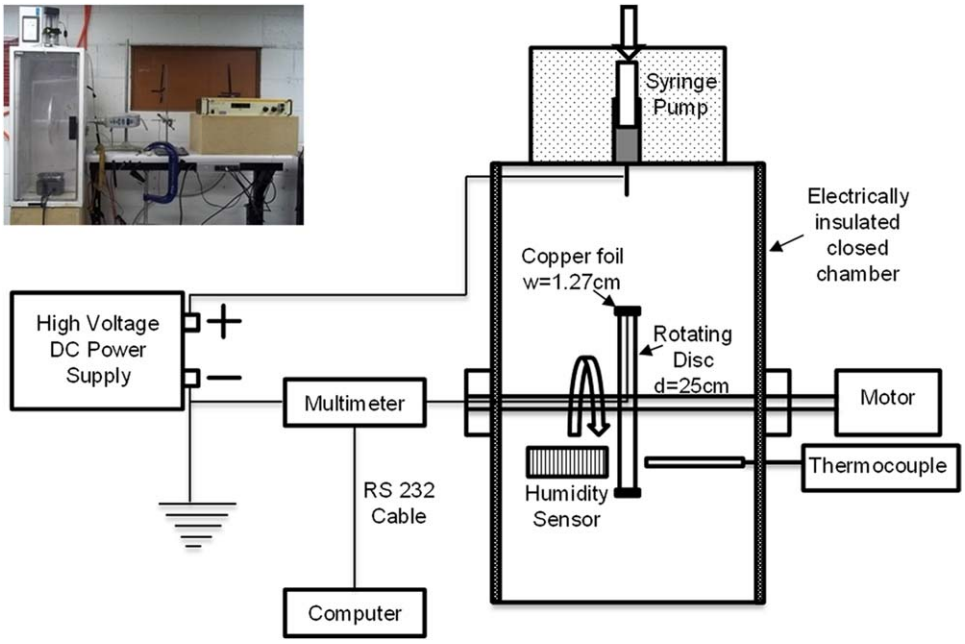

Figure 1. Schematic of the experimental set-up for electrospinning using vertical feeding syringe pump and rotating disk collector inside an electrically insulated chamber. Insert shows a picture of the set-up used. [Color figure can be viewed in the online issue, which is available at wileyonlinelibrary.com.]

Electronics Corporation. A copper foil (width 1.27 cm) was glued on the surface of a 25 cm diameter plastic disc collector. The distance between the tip of the needle and the upper surface of the disk was kept constant at 18 cm. The copper foil on the disc surface was electrically connected to the ground. Electrospinning was carried out by applying a positive high voltage to the needle while the disc was rotating at 600 rpm to produce aligned fibers in the direction of rotation. The solution flow rate was maintained using a positive displacement syringe pump (KDS 200) purchased from KD Scientific Inc. About 200 μl solution was deposited on the disc. All electrospun nanofibers were collected at 20°C and 30% RH. The electrospun nanofiber bundles were peeled off from the copper foil in the form of yarn after immerging in distilled water. The yarns were then mounted on a drying rack to keep them in tension and dried at 95°C for 5 h. Photographs of the PAN nanofiber yarns showing peeling off the disc and drying rack with nanofiber yarn mounted are shown in Figure 2.

Characterization Techniques

An optical camera was used to visually observe the Taylor cone region during the electrospinning process. ImageJ software was used to process and convert the optical images to binary images. An example of optical image and its binary image of Taylor cone is depicted in Figure 3. The charge carried by the polymer solution jet, defined as fiber current, was measured by a multimeter placed between the collector and the ground (Figure 1). A RS232 cable connected to a computer along with a data logger software was used to read the current signal. The accuracy of the current measurement was validated by adding a simple circuit of a known voltage (1.56 V) and a known resistance in series. By changing the resistance (2∼20 MΩ) various theoretical current can be estimated. The actual current in the circuit was then measured using the multimeter via RS232 cable. Figure 4 shows the variation in multimeter reading as a function of time during an open circuit and a 163.8 nA theoretical current measurement. During the open circuit measurement, the multimeter reading

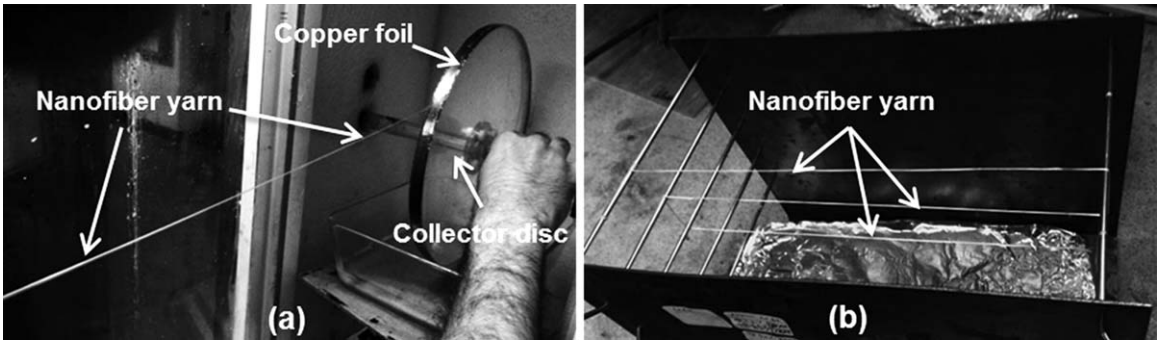

Figure 2. Photographs showing (a) peeling off the PAN nanofiber yarn from the copper foil on the rotating disc and (b) drying rack with nanofiber yarns mounted.

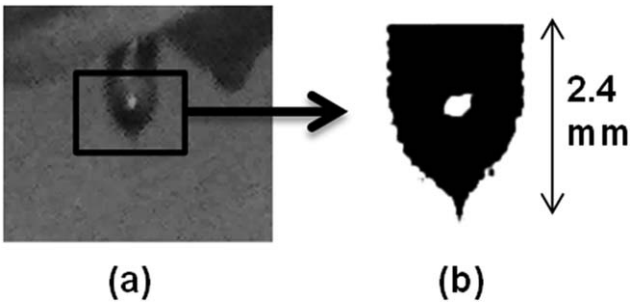

Figure 3. Optical image of the Taylor cone region (a) and its binary image (b) after processing using ImageJ software.

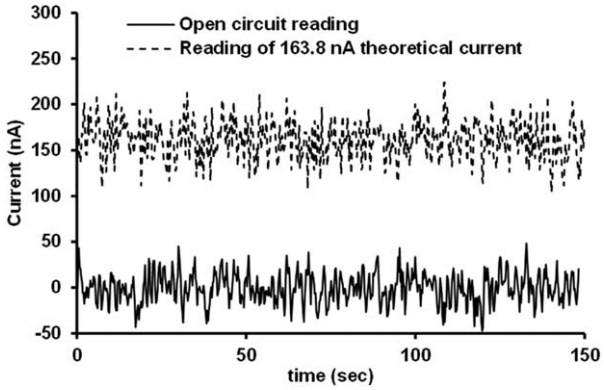

Figure 4. Open circuit and 163.8 nA theoretical current reading of the multimeter.

varies within +/- 50 nA (Figure 4, bottom curve) which is due to the accuracy limitation of the multimeter. Since multimeter reading accuracy is specified on a "per measurement point" the average value of the current readings for a range of time represent the actual current value. However, a normality test should be done for a range of time to verify the multimeter reading. Figure 5 shows the Anderson-darling normality test results of the current reading shown in Figure 4. In both cases P-value is greater than 0.05 which means the data is normal. The corresponding average current readings from the multimeter are compared with the theoretical values for three external resistances as shown in Table I. Both theroretical and percent errors are also indicated. As seen from Table I that all measurement errors are less than 2% of the theoretical current value which indicates that the average current value of the multimeter reading for any range of time represents the actual measured current. The morphology of the electrospun nanofibers were observed by scanning electron microscope (SEM). Nanofiber yarns were mounted on the SEM sample holder, sputter coated with Iridium, and examined using a Zeiss Neon high resolution SEM. Dynamic mechanical analyzer (DMA) Q800 from TA Instruments was utilized to perform the tensile experiments. Nanofiber yarns were directly mounted on the DMA grip and aligned before applying any load. All tensile tests were performed at room temperature with a sample gauge length of 9–10 mm and at constant strain rate of 0.001 s^{-1}. The cross-sectional area of the yarn sample was calculated by dividing the mass of the yarn by its length and density of PAN. The density of the PAN is assumed to be 1.18 g/cc.

RESULTS AND DISCUSSION

Taylor Cone Morphology and Fiber Current

During electrospinning process the polymer solution near the Taylor cone may appear in many forms depending on the process conditions. In this study, we investigate the Taylor cone at the tip of the needle at different flow rates and field strengths using an optical camera. Figure 6(a) shows various Taylor cone morphologies observed at different flow rates at 15 kV electric field. Based on the morphologies shown jets are characterized as (a) dripping, (b) jet with intermittent drops, (c) continuous jet, and (d) discontinuous jet. Each Taylor cone morphology is also classified into a regime. At high flow rate (i.e., 32 μL/min), the electric field is not sufficient enough to overcome the surface tension of the fluid, hence the fluid accumulates at the tip of the needle and eventually falls in drops (regime 1: dripping). With decreasing the flow rate, an emerged liquid jet can be found, however the electric field strength and charge density is still low at which the rate of fluid removal can't match with the rate of supply. Thus the nanofiber deposition is accompanied by intermittent droplets as shown in regime 2: jet with intermittent drops. Decreasing the flow rate below a critical value results in a continuous jet, however there is a large variation of the Taylor cone morphology observed in this region (i.e. regime 3) of flow rate. In this region a slight variation of the flow rate can significantly affect the Taylor cone morphology and the spinning jet. The flow rate corresponds to regime 4 lead to stable operation

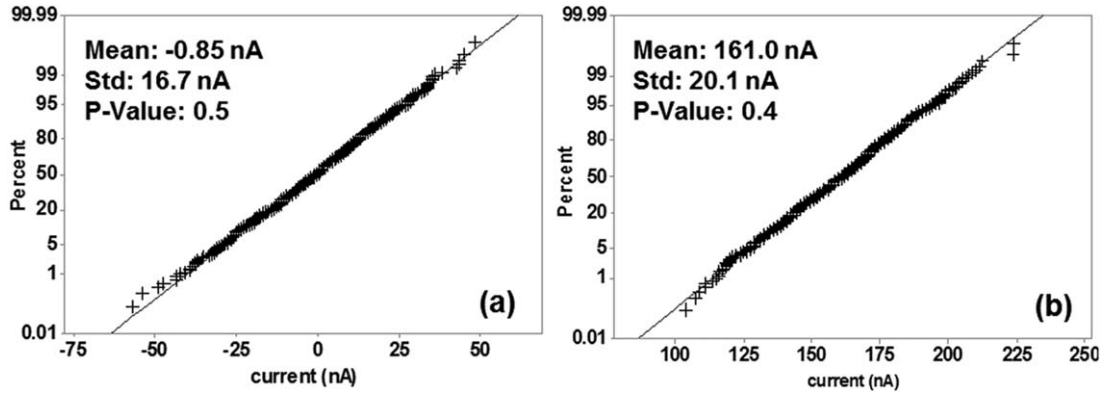

Figure 5. Anderson-darling normality test for the data shown in Figure 4. (a) Open circuit reading, (b) 163.8 nA theoretical current reading.

Table I. Comparison Between Estimated Theoretical Current and Experimentally Determined Current

Theoretical current (nA)	Experimental current (nA)	Deviation (%)
0 (open circuit)	−0.9	–
80.2	81.3	1.3
163.8	161	1.7
688.7	701.8	1.9

for a long period of time with minimal deviation. A slight decrease in the flow rate makes the Taylor cone region narrower and variable jet (continuous jet - regime 5), and eventually reach to a point where the jet is no more continuous (discontinuous jet - regime 6). We have also studied the half angle of the Taylor cone, i.e. the sharpness of the hyperboloid shape to analyze the stability of the jet at various regimes. It has been reported in the literature that the half-angle (α) of the Taylor cone often lies in the range of $32° < \alpha < 46°$[57,58] for stable jet. However, Yarin *et al.*[59] theoretically predicted that the droplet approaches a conical asymptotic with a half-angle of 33.5° when the electric field reaches its critical value. The experimental value of their half-angle for stable Taylor cone was 37°, very close to the predicted value. We have also measured half-angles of the Taylor cone for selected flow regimes such as regimes 2, 3, 4, and 5 and the values are also shown in Figure 6(b). The corresponding half-angles are found to be about 47°, 45.5°, 35.5°, and 23.5° for regime 2, regime 3, regime 4, and regime 5, respectively. It should be noted that the half angle for each flow rate is not a constant number and varies depending on the stability of the jet, thus the variation is very small in regime 3 as compared to other regimes. The half-angles for regime 2 and 5 are outside the stability range according to the reported values in the literature ($32° < \alpha < 46°$)[57,58] and ($\alpha = 33.5°$).[59] Higher value of the half-angle in regime 2 indicates that the electrical potential is not high enough to keep up with the flow rate and eventually, falling into drops. Although regime 5 yielded continuous jet, the half-angle was found much lower (~23.5°) than the predicted value of 33.5° which also makes the jet unstable. With decreasing the flow rate the intermittent falling of the drops was prevented (regime 3), and half-angle of the Taylor cone was reduced (around 45.5°) and fall in the range of $32° < \alpha < 46°$. However, this angle is much higher than the predicted value of 33.5°, which we believe to be the reason for jet instability. The half-angle in regime 4 was found to be around 35.5° which is very close to the predicted and experimentally determined values by Yarin *et al.*[59] for stable electrospinning process. The half-angle value should maintain close to this number as long as the solution flow rate to the Taylor cone match with the solution leaving the Taylor cone, and we believe that the corresponding flow rate in regime 4 makes the electrospinning process more stable compared to other flow rates.

Similar analysis was performed at different electric field strengths to determine the upper and lower bound of flow rates for continuous jet operation as shown in Figure 7. The flow rate for continuous jet operation was found to increase with increasing field strength. However, the slope of the upper bound flow rate curve is much higher compared to the lower bound flow rate resulting in increase in operational window of the flow rate with the increase of the electrospinning voltage.

It was reported in the literature that the fiber current measurement can provide useful information about the deposition during the electrospinning process.[51,52] In this study, the fiber current was measured to investigate fiber deposition state at different flow rates and applied voltages. Figure 8 shows the

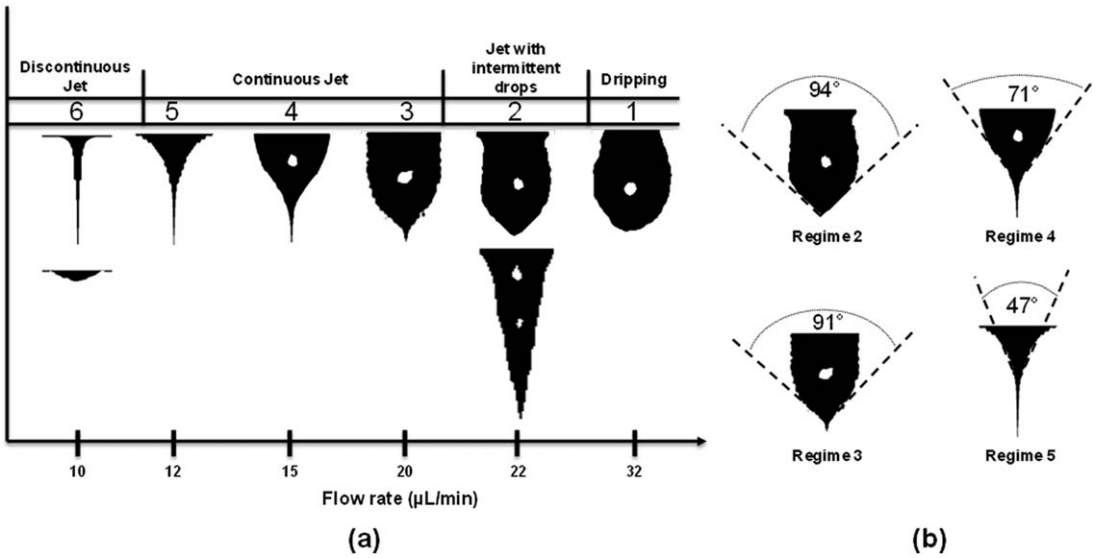

Figure 6. (a) Various Taylor cone morphologies observed at different flow rates operating at 15 kV electric field. (1) Dripping, (2) Jet with intermittent drops (bottom: change in Taylor cone shape right at the time of drop falling), (3) continuous jet with large, bounded variations, (4) continuous jet with minimal fluctuations, (5) narrow, variable continuous jet, (6) discontinuous jet (top), no jet (bottom). (b) Taylor cone angles for various regimes of interest (Regime 2−5).

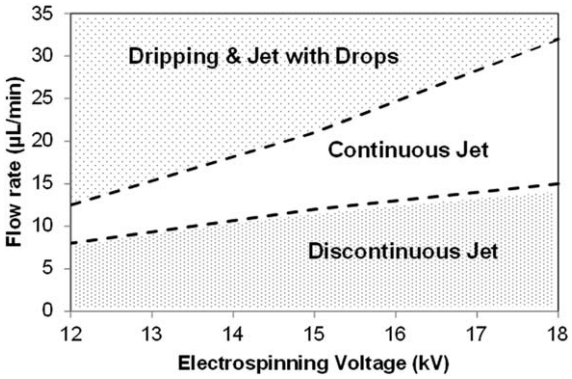

Figure 7. Dependence of upper and lower bounds of flow rate on electric field for continuous jet operation.

variation of the instantaneous fiber current measured at different flow rates at 15 kV electric field. As shown, at 1 μL/min flow rate [Figure 8(a)], the fiber current was mostly zero except some intermittent sharp peaks. Due to a very low flow rate there was not enough solution at the tip of the needle to eject a jet, resulting in no fiber deposition. Once enough solution accumulates at the tip of the needle, the liquid jet ejects from the needle in the form of fiber and deposit on the collector surface. At 5 μL/min flow rate, an intermittent continuous jet condition was achieved as seen from Figure 8(b) where the electrospinning jet stayed continuous for about 20 s. The inset pictures show zero fiber current when there is no jet ejection and about 160 nA current when jet is ejected from the needle. At 10 μL/min [Figure 8(c)], the fiber current with very sharp intermittent peaks (150 nA to zero) indicates that the electrospinning jet was in the verge of getting continuous. At 12 μL/min flow rate, a continuous jet was achieved with fiber current not dropping to zero, as shown in Figure 8(d). A few minor drops in fiber current from 150 nA to 50 nA is an indication of narrow and variable Taylor cone, as shown in Figure 6. No fluctuation in fiber current was observed at 15 μL/min [Figure 8(e)] as expected from visual observation of the Taylor cone (Figure 6). Although there was fluctuation in the Taylor cone volume (Figure 6) at 20 μL/min, no sharp peaks in the fiber current was observed [Figure 8(f)]. Sharp downward peaks in the fiber current at low flow rates are indication of huge drop in the amount of fiber deposition rate. At higher flow rate, the fiber deposition rate may vary as the volume of the Taylor cone changes; however the total charge carried by the liquid jet did not cause any significant variation in the fiber current.

Diameter Distribution of Electrospun Nanofibers

PAN nanofibers were fabricated at different electric fields (12 kV, 15 kV, and 18 kV) and flow rates (5 μL/min to 28 μL/min) covering both continuous and discontinuous jet regimes. A few SEM images and corresponding diameter distributions of PAN nanofibers produced at 15 kV electric field are shown in Figure 9 for continuous jet conditions and in Figure 10 for discontinuous jet conditions. As shown, at 15 μL/min and 17 μL/min flow rates the fibers are found to have smaller average diameter and narrower diameter distribution as well as uniform surface morphology. Similar observations are also found at 20 μL/min flow rate for 18 kV and at 10 μL/min flow rate for 12 kV. For other conditions (continuous and discontinuous jet regimes), the nanofibers show larger average diameter and wider diameter distribution. It is believed that the electrospinning parameters that yield a stable Taylor cone produces uniform and smaller diameter fibers.

Effect of Electric Field and Flow Rate on Nanofiber Diameter

Figure 11 shows the variation of average nanofiber diameter as a function of flow rate for 15 kV and 18 kV electric fields. It can be seen that at both electric fields, the fiber diameter

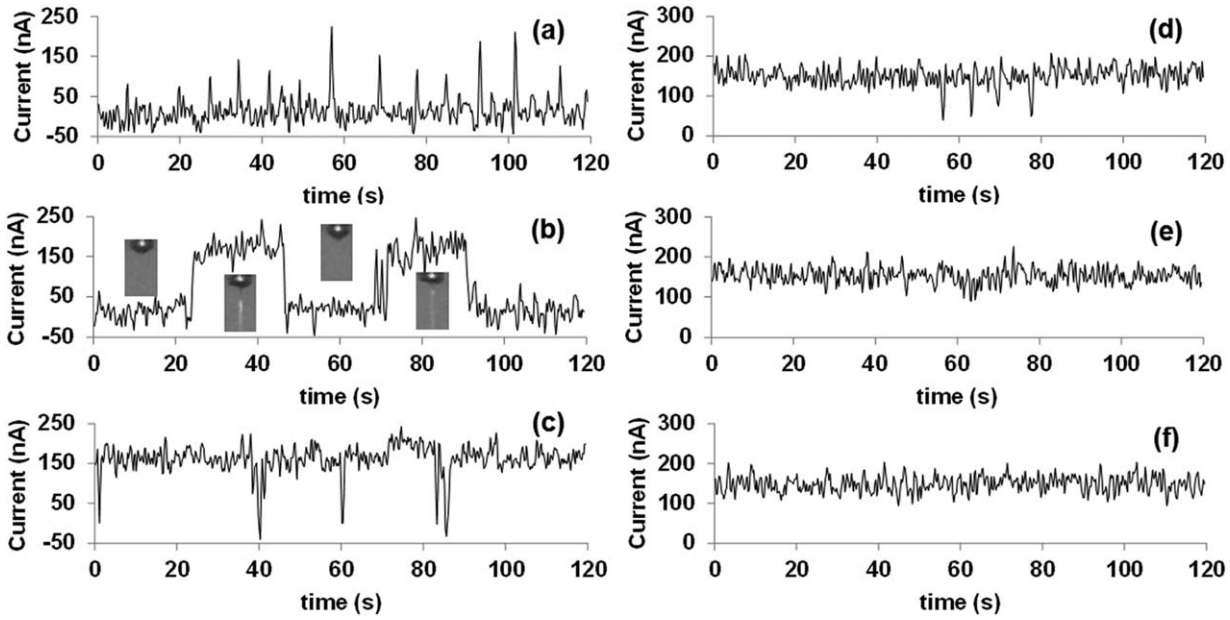

Figure 8. Instantaneous fiber current at different flow rates operating at 15 kV electric field: (a) 1 μL/min, (b) 5 μL/min (inset pictures show intermittent jet ejection), (c) 10 μL/min, (d) 12 μL/min, (e) 15 μL/min, and (f) 20 μL/min.

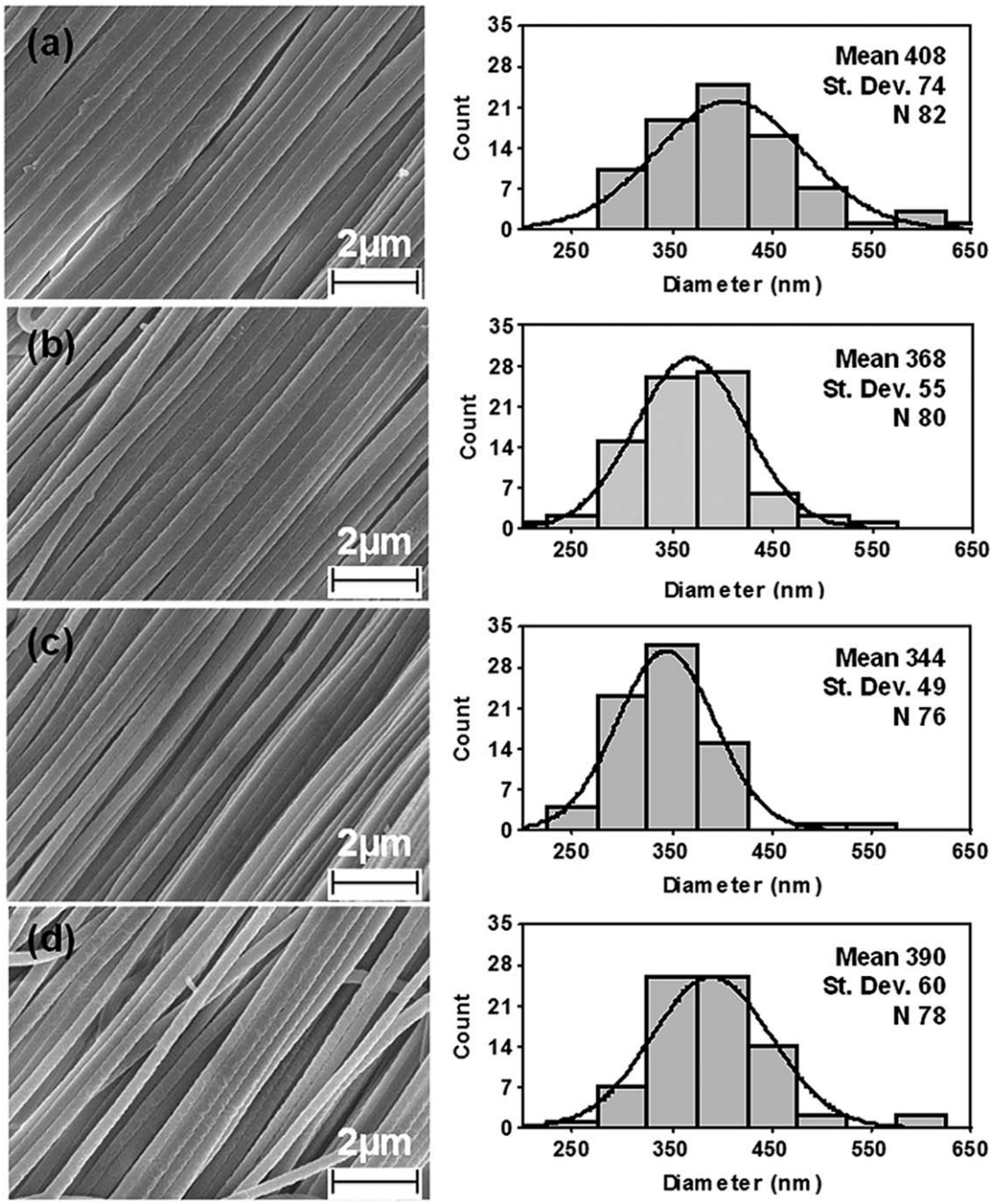

Figure 9. SEM micrographs of PAN nanofibers and corresponding diameter distribution for 15 kV and at various flow rates in the regime of continuous jet. (a) 20 μL/min, (b) 17 μL/min, (c) 15 μL/min, and (d) 12 μL/min.

reaches to a minimum value before increasing with further increase in the flow rate. The condition at which the fiber diameter reaches to a minimum value can be called as "favorable flow rate". As seen from figure the favorable flow rate is about 15 μL/min at 15 kV and is about 20 μL/min at 18 kV. Thus, it can be stated that the favorable flow rate is higher at higher applied voltage which has a physical significance. For example, higher production rate of nanofibers can be achieved by adopting higher favorable flow rate corresponds to higher electrospinning voltage.

Mechanical Properties of PAN Nanofiber Yarns

Effect of Filament Diameter. In this study, we select three PAN nanofiber yarns with different average filament diameter. All PAN nanofiber yarns were fabricated using flow rates and electric voltages within the continuous flow regime. Typical tensile stress vs strain of selected PAN nanofiber yarns with different average filament diameter are shown in Figure 12. As seen both tensile strength and modulus increase as the filament diameter deceases in the yarn. It is expected that the alignment of the polymer chains/molecules increases with diameter decreases due

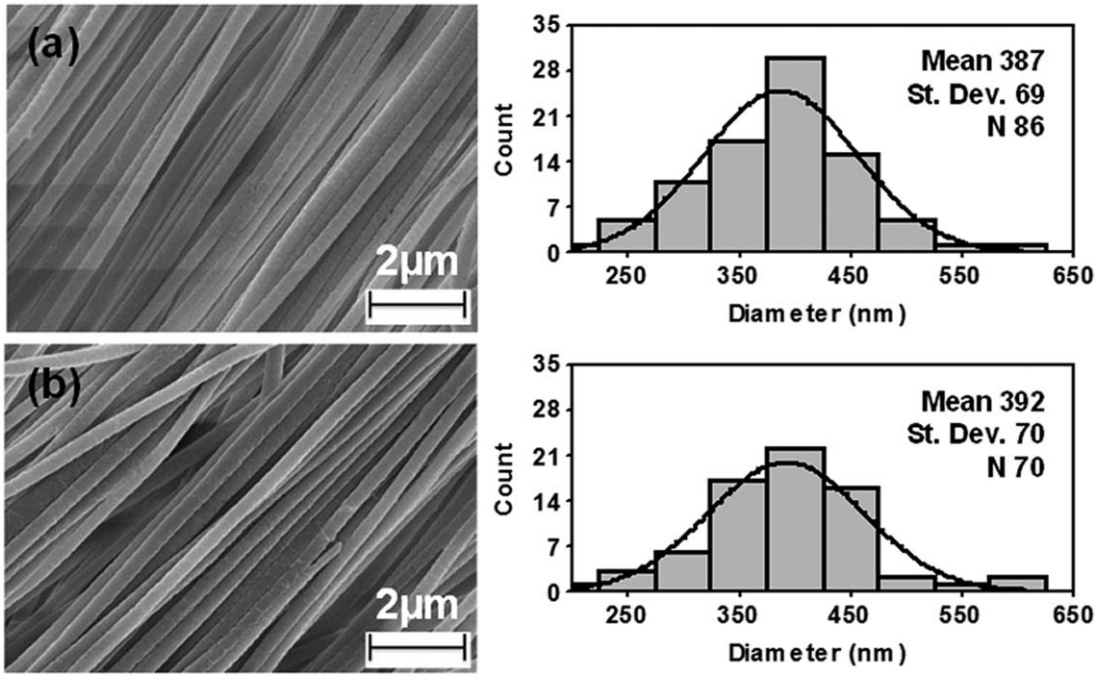

Figure 10. SEM micrographs of PAN nanofibers and corresponding diameter distribution for15 kV and at various flow rates in the regime of discontinuous jet. (a) 10 μL/min, and (b) 5 μL/min.

to stretching of the fiber during the electrospinning process. However, interestingly, the strain at break and toughness were found to increase with decrease in filament diameter. Based on classical behavior of the structural materials, one would expect strain at failure and toughness to decrease as strength and modulus increase. The unusual behavior of electrospun nanofibers was also observed by Papkov *et al.*[53] They found that the degree of crystallinity of the nanofiber decreased with decrease of nanofiber diameter. According to them, low crystallinity of electrospun nanofiber may be the result of fast solvent evaporation from electrospun jets leading to rapid jet solidification. As smaller jets lose more solvent and solidify quicker, the degree of crystallinity is lower for yarns with lower nanofiber diameter resulting in higher strain at break and toughness. Higher diameter nanofibers will have more time for solvent evaporation and hence polymer molecules will have enough time to form crystallization. Moreover, exhaustion of solvent may not occur completely and some solvent molecule may be trapped under the solidified skin which may results in more voids in the larger diameter fiber and therefore, lower strength and strain in break was observed.

Continuous Jet vs. Discontinuous Jet. In this study, we select a few nanofiber yarns with similar filament diameter fabricated using both continuous and discontinuous jet conditions. Typical tensile stress-strain plots of a few nanofiber yarns produced from continuous jet and discontinuous jet conditions having similar filament diameter are shown in Figure 13. Toughness values for each type of yarns are also included in the figure. As seen from Figure 13, yarns produced from discontinuous jet exhibit lower tensile properties (strength, strain, and toughness)

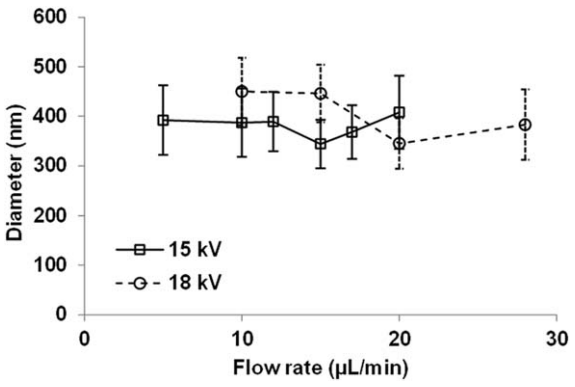

Figure 11. Variations in average nanofiber diameter as a function of flow rates for 15 kV and 18 kV electric fields.

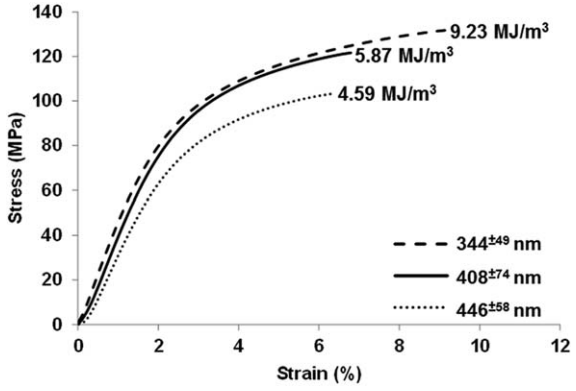

Figure 12. Effect of filament diameter on tensile stress-strain behavior of PAN nanofiber yarns made from continuous jet conditions. Toughness was calculated from the area under the stress−strain curves.

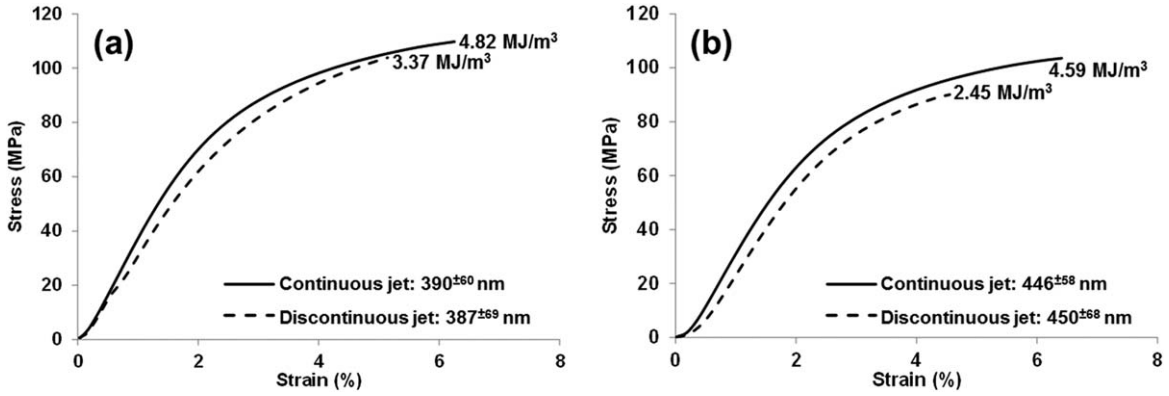

Figure 13. Stress−strain plots of PAN nanofiber yarns having similar filament diameter produced from continuous and discontinuous jet conditions. Toughness was calculated from the area under the stress−strain curves.

compared to yarns produced from continuous jet. It is believed that the nanofiber yarns made from discontinuous jet consist of filaments with shorter in length and as a result they are less effective in transferring load from filament to filament. Yarns with longer filament are more effective in load transferring, and as a result show higher tensile properties.

Effect of Flow Rate. Figure 14 shows the variation of tensile strength of PAN yarns as a function of flow rate at different electric fields. Filled and non-filled symbols correspond to nanofiber produced using continuous jet and discontinuous jet, respectively. Their corresponding average filament diameters are also included in the figure. As shown in Figure 14, PAN yarns made at flow rates in the discontinuous jet regime exhibit lower tensile strength. With increasing flow rate the jet condition becomes continuous and yarns show higher tensile strength up to a point beyond further increase in the flow rate decreases the tensile strength. The highest tensile strengths were found at 15 μL/min for 15 kV and at 20 μL/min for 18 kV. These conditions also yield PAN yarns with lowest filament diameter and other conditions result in larger diameter fibers due to excessive pooling of PAN solution and hence lower tensile properties.

Modeling of the Nanofiber Diameter

The dependence of nanofiber diameter on electrospinning voltage and flow rate cannot be isolated, rather they are unified and their combined effect can be defined in terms of volume charge density (I/Q). Fridrikh *et al.*[60] developed a simple model to correlate the fiber diameter with the volume charge density by analyzing the dynamic equations, describing the motion of whipping jet of Hohman.[61,62] Evaluating the asymptotic balance between normal stresses due to surface tension and surface charge repulsion, the relationship can be written as:

$$d_{\text{fiber}} = c^{1/2}\left(\gamma\varepsilon\frac{Q^2}{I^2}\frac{2}{\pi(2\ln\chi-3)}\right)^{1/3}$$

where c is the polymer concentration; γ is the surface tension (N/m); ε is the dielectric constant of ambient air; Q is the flow rate (m^3/s); I is the measured fiber current (A); χ is the dimensionless wavelength of the instability response for the normal displacements. Volume charge density (I/Q) has a unit of C/m^3 and hence it means the strength of the electrostatic force acting on the jet. It is expected that the fiber diameter is proportional to $(I/Q)^{-2/3}$ as other parameters remain constant. Thus, the average nanofiber diameter expected to decrease with increase in the volume charge density. Cai and Gevelber.[46] confirmed this analysis for Polyethylene oxide (PEO) aqueous solution; however, it is to be mentioned that this relationship holds true only if the flow rate represents stable regime of the Taylor cone and the relative humidity remains constant.

For verification, we plotted average nanofiber diameter with the volume charge density (I/Q) for four electrospinning conditions,

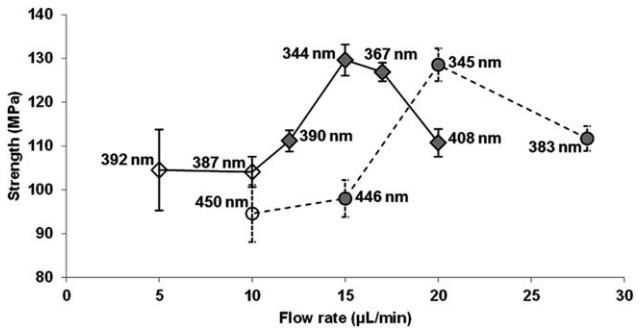

Figure 14. Variation of tensile strength of PAN nanofiber yarns as a function of flow rate at different electrospinning voltage. Filled, continuous jet; nonfilled, discontinuous jet.

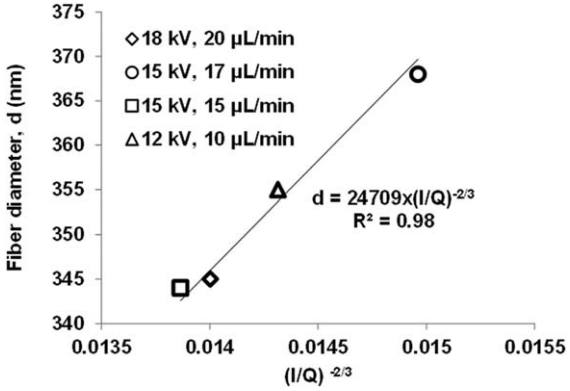

Figure 15. Correlation between the average nanofiber diameter and volumetric charge density (I/Q)−2/3.

where spinning jet was continuous and Taylor cone was stable, as shown in Figure 15. As seen from the figure the relationship between the fiber diameter and $(I/Q)^{-2/3}$ is very linear. Thus, it can be concluded that the electrospinning voltage and the flow rate affect the nanofiber diameter as a combined effect and can be used as a predicting tool for design of electrospinning process for nanofiber fabrication with improved mechanical performance.

CONCLUSIONS

This paper investigates the effects of the electric field and flow rate on the diameter of electrospun PAN nanofiber and tensile properties of nanofiber yarns. By investigating the Taylor cone morphology at the tip of the needle, a favorable flow regime with minimal jet fluctuation can be determined. Yarns made using favorable flow conditions yield uniform and thinner nanofiber exhibiting higher tensile strength, modulus, and toughness. A simple model that combines the effect of voltage and flow rate in terms of volume charge density (I/Q) was adopted, and a linear relationship between the mean nanofiber diameter and $(I/Q)^{-2/3}$ was found. Using this relationship the electrospinning process can be designed to produce uniform nanofibers with superior mechanical performance for achieving higher production rate of the nanofibers.

ACKNOWLEDGMENTS

The authors thank M. Cengiz Altan for high voltage power supply, Carl B. Van Buskirk and Chad E. Cunningham for assisting with high voltage power cables. They also thank Anandh Balakrishnan for his initial involvement in this project.

REFERENCES

1. Ondarcuhu, T.; Joachim, C. *Europhys. Lett.* **1998**, *42*, 215.
2. Fu, X.; Li, F.; Liu, W.; Stefanini, C.; Dario, P. *Microelectron. Eng.* **2011**, *88*, 2653.
3. Feng, L.; Li, S.; Li, H.; Zhai, J.; Song, Y.; Jiang, J.; Zhu, D. *Angew. Chem.* **2002**, *114*, 1269.
4. Martin, C. R. *Chem. Mater.* **1996**, *8*, 1739.
5. Ma, P. X.; Zhang, R. *J. Biomed. Mat. Res.* **1999**, *46*, 60.
6. Whitesides, G. M.; Grzybowski, B. *Science* **2002**, *295*, 2418.
7. Liu, G. J.; Ding, J. F.; Qiao, L. J.; Guo, A.; Dymov, B. P.; Gleeson, J. T.; Hashimoto, T.; Saijo, K. *Chem.-A Eur. J.* **1999**, *5*, 2740.
8. Bhardwaj, N.; Kundu, S. C. *Biotechnol. Adv.* **2010**, *28*, 325.
9. Doshi, J.; Reneker, D. H. *J. Electrostat.* **1995**, *35*, 151.
10. Reneker, D. H.; Yarin, A. L.; Fong, H.; Koombhongse, S. *J. Appl. Phys.* **2000**, *87*, 4531.
11. Feng, J. J. *Phys. Fluids* **2002**, *14*, 3912.
12. Huang, Z. M.; Zhang, Y. Z.; Kotaki, M.; Ramakrishna, S. *Compos. Sci. Technol.* **2003**, *63*, 2223.
13. Ramakrishna, S.; Fujihara, K.; Wee-Eong, T.; Yong, T.; Ma, Z.; Ramaseshan, R. *Mater. Today* **2006**, *9*, 40.
14. Gupta, P.; Elkins, C.; Long, T. E.; Wilkes, G. L. *Polymer* **2005**, *46*, 4799.
15. Theron, S.; Zussman, E.; Yarin, A. L. *Polymer* **2004**, *45*, 2017.
16. Geng, X.; Oh-Hyeong, K.; Jang, J. *Biomaterials* **2004**, *26*, 5427.
17. Fong, H.; Chun, I.; Reneker, D. H. *Polymer* **1999**, *40*, 4585.
18. Ashraf, A. A.; El-Hamid, M. A. *Compos. Part A: Appl. S.* **2006**, *37*, 1681.
19. Heikkilä, P.; Harlin, A. *Eur. Polym. J.* **2008**, *44*, 3067.
20. Zhang, C.; Yuan, X.; Wu, L.; Han, Y.; Sheng, J. *Eur. Polym. J.* **2005**, *41*, 423.
21. Teo, W. E.; Ramakrishna, S. *Nanotechnology* **2006**, *17*, R89.
22. Pham, Q. P.; Sharma, U.; Mikos, A. G. *Tissue Eng.* **2006**, *12*, 1197.
23. Pelipenko, J.; Kristl, J.; Janković, B.; Baumgartner, S.; Kocbek, P. *Int. J. Pharm.* **2013**, *456*, 125.
24. Vrieze, S. D.; Camp, T. V.; Nelvig, A.; Hangstrom, B.; Westbroek, P.; Clerck, K. D. *J. Mater. Sci.* **2009**, *44*, 1357.
25. Lee, K. H.; Kim, H. Y.; Bang, H. J.; Jung, Y. H.; Lee, S. G. *Polymer* **2003**, *44*, 4029.
26. Lee, J. S.; Choi, K. H.; Ghim, H. D.; Kim, S. S.; Chun, D. H.; Kim, H. Y.; Lyoo, W. S. *J. Appl. Polym. Sci.* **2004**, *93*, 1638.
27. Demir, M. M.; Yilgor, I.; Yilgor, E.; Erman, B. *Polymer* **2002**, *43*, 3303.
28. Mckee, M. G.; Wilkes, G. L.; Colby, R. H.; Long, T. E. *Macromolecules* **2004**, *37*, 1760.
29. Jiang, H.; Fang, D.; Hsiao, B. S.; Chu, B.; Chen, W. *Biomacromolecules* **2004**, *5*, 326.
30. Huang, L.; Nagapudi, K.; Apkarian, R. P.; Chaikof, E. L. *J. Biomater. Sci. Polym. E.* **2001**, *12*, 979.
31. Zuo, W. W.; Zhu, M. F.; Yang, W.; Yu, H.; Chen, Y. M.; Zhang, Y. *Polym. Eng. Sci.* **2005**, *45*, 704.
32. Li, Y.; Huang, Z.; Lu, Y. *Eur. Polym. J.* **2006**, *42*, 1696.
33. Yuan, X. Y.; Zhang, Y. Y.; Dong, C. H.; Sheng, J. *Polym. Int.* **2004**, *53*, 1704.
34. Zong, X. H.; Kim, K.; Fang, D. F.; Ran, S. F.; Hsiao, B. S.; Chu, B. *Polymer* **2002**, *43*, 4403.
35. Du, J.; Shintay, S.; Zhang, X. J. *Polym. Sci. B Polym. Phys.* **2008**, *46*, 1611.
36. Zhang, C. X.; Yuan, X. Y.; Wu, L. L.; Han, Y.; Sheng, J. *Eur. Polym. J.* **2005**, *41*, 423.
37. Yördem, O. S.; Papila, M.; Menceloglu, Y. Z. *Mater. Des.* **2008**, *29*, 34.
38. Buchko, C. J.; Chen, L. C.; Shen, Y.; Martin, D. C. *Polymer* **1999**, *40*, 7397.
39. Megelski, S.; Stephens, J. S.; Chase, D. B.; Rabolt, J. F. *Macromolecules* **2002**, *35*, 8456.
40. Du, J.; Shintay, S.; Zhang, X. *J. Polym. Sci. Polym. Phys.* **2008**, *46*, 1611.
41. Baumgarten, P. K. *J. Colloid Interf. Sci.* **1971**, *36*, 71.
42. Tan, S.-H.; Inai, R.; Kotaki, M.; Ramakrishna, S. *Polymer* **2005**, *46*, 6128.
43. Ki, C. S.; Baek, D. H.; Gang, K. D.; Lee, K. H.; Um, I. C.; Park, Y. H. *Polymer* **2005**, *46*, 5094.

44. Geng, X. Y.; Kwon, O. H.; Jang, J. H. *Biomaterials* **2005**, *26*, 5427.
45. Reneker, D. H.; Yarin, A. L. *Polymer* **2008**, *49*, 2387.
46. Cai, Y.; Gevelber, M. *J. Mater. Sci.* **2013**, *48*, 7812.
47. Fennessey, S. F.; Farris, R. J. *Polymer* **2004**, *12*, 4217.
48. Fitzer, E. Carbon Reinforcements and Carbon/Carbon Composites. Springer: New York, 1998; Chapter 1, p 3.
49. Nasouri, K.; Bahrambeygi, H.; Rabbi, A.; Shoushtari, A. M.; Kaflou, A. *J. Appl. Polym. Sci.* **2012**, *126*, 127.
50. Basu, S.; Agrawal, A. K.; Jassal, M. *J. Appl. Polym. Sci.* **2011**, *122*, 856.
51. Samatham, R.; Kim, K. *J. Polym. Eng. Sci.* **2006**, *46*, 954.
52. Fallahi, D.; Refizadeh, M.; Mohammadi, N.; Vahidi, B. *Polym. Int.* **2008**, *57*, 1363.
53. Papkov, D.; Zou, Y.; Andalib, M. N.; Goponenko, A.; Cheng, S. Z. D.; Dzenis, Y. A. *ACS Nano* **2013**, *7*, 3324.
54. Molnar, K.; Vas, L. M.; Czigany, T. *Compos. Part B-Eng.* **2012**, *43*, 15.
55. Moon, S.; Farris, R. J. *Carbon* **2009**, *47*, 2829.
56. Hou, H.; Ge, J. J.; Zeng, J.; Li, Q.; Reneker, D. H.; Greiner, A.; Cheng, S. Z. *Chem. Mater.* **2005**, *17*, 967.
57. Mora, J. F. D. L. *J. Fluid Mech.* **1992**, *243*, 561.
58. Yu, D.; Williams, G. R.; Wang, X.; Liu, X.; Li, H.; Bligh, S. W. A. *RSC Adv.* **2013**, *3*, 4652.
59. Yarin, A. L.; Koombhongse, S.; Reneker, D. H. J. *Appl. Phys.* **2001**, *90*, 4836.
60. Fridrikh, S. V.; Jian, H. Y.; Brenner, M. P.; Rutledge, G. C. *Phys. Rev. Lett.* **2003**, *90*, 144502.
61. Hohman, M. M.; Shin, M.; Rutledge, G.; Brenner, M. P. *Phys. Fluids* **2001**, *13*, 2201.
62. Hohman, M. M.; Shin, M.; Rutledge, G.; Brenner, M. P. *Phys. Fluids* **2001**, *13*, 2221.